Inorganic Chemistry

Article

pubs.acs.org/IC

A Theoretical Study of Metal–Metal Cooperativity in the Homogeneous Water Gas Shift Reaction

Nishamol Kuriakose, Shantanu Kadam, and Kumar Vanka*

National Chemical Laboratory (NCL), Dr. Homi Bhabha Road, Pashan, Pune 411008, Maharashtra, India

Supporting Information

ABSTRACT: The possibility of metal–metal cooperativity in improving the yield of the homogeneous water gas shift reaction (WGSR) has been investigated through full quantum mechanical density functional theory calculations. The calculations indicate that bimetallic catalysts would be likely to be more highly active than mononuclear metal-based catalysts for the WGSR. The results have implications for the design of improved WGSR catalysts in the future.

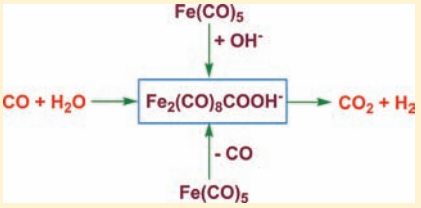

INTRODUCTION

The presence of two metal centers in an organometallic complex can give rise to interesting new chemistry because of the interaction and cooperativity between the metal centers. This has led to a conscious effort in recent years to create binuclear metal complexes and investigate their impact on important catalytic reactions such as olefin polymerization,[1] C–H activation,[2] and alkyne/methylene coupling reactions.[3] However, the fact that binuclear complexes confer advantages in homogeneous catalysis systems due to metal–metal cooperativity leads to an important question: is it possible that reactions that have been considered to date to occur at mononuclear metal centers *could be happening instead at binuclear centers, with the binuclear species being formed during the homogeneous catalysis process?*

An interesting reaction in this regard is the homogeneous water gas shift reaction (WGSR).[4−10] The WGSR has significance in industrial applications because it improves the hydrogen content of water gas, thereby enhancing the steam reforming process as shown in equations 1 and 2. Also, the WGSR has implications in the conversion of biomass to hydrocarbons[11−13] and can thus have an impact in resolving the energy crisis. The homogeneous catalysis of the WGSR is important because it requires milder conditions,[14] with water being present as a liquid, than the heterogeneous catalysis systems, which have traditionally been used in industry. Therefore, there has been considerable interest in recent years toward understanding the mechanism of the WGSR for homogeneous catalysis systems. Transition metal carbonyls[14,15] such as $Cr(CO)_6$ and $Mo(CO)_6$ have been employed as homogeneous catalysts of the WGSR, but it is $Fe(CO)_5$ that has been used in almost all experimental and computational studies that have focused on understanding the mechanism of the WGSR. Several groups have proposed different mechanistic cycles for the $Fe(CO)_5$-catalyzed WGSR.

$$CH_4 + H_2O \rightarrow CO + H_2 + CO_2 \quad (1)$$

$$CO + H_2O \rightarrow CO_2 + H_2 \quad (2)$$

From experimental observations, a gas-phase $Fe(CO)_5$-catalyzed WGSR was initially proposed to proceed through a catalytic cycle, as shown in Scheme 1, which included the experimentally substantiated individual reactions.[16] Subsequent modifications to the mechanism were proposed by Sunderlin and Squires,[17] who suggested a $Fe(CO)_4COOH^-$ intermediate,[18] based on new experimental observations. Torrent et al.[19] investigated this mechanism through a theoretical approach and proposed a $[H_2O]$-$[Fe(CO)_4H^-]$ adduct followed by OH^- desorption to yield the $Fe(CO)_4H_2$ species (see Scheme 2). Because this OH^- desorption step was found to have a high energy barrier, Barrows[20] suggested a further modification that avoided this step by having the $Fe(CO)_4COOH^-$ species directly convert to $Fe(CO)_4CHO^-$ and back to $Fe(CO)_4COOH^-$ (see Scheme 3). However, because the Barrows mechanism avoided the experimentally observed $Fe(CO)_4H^-$ species, Rozanska and Vuilleumier[21] proposed

Scheme 1. Mechanism Initially Proposed for the $Fe(CO)_5$-Catalyzed WGSR

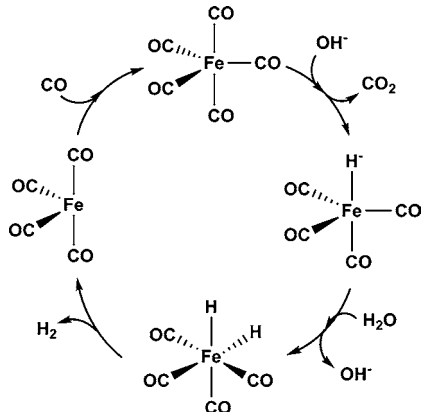

Received: August 17, 2011
Published: December 8, 2011

   dx.doi.org/10.1021/ic201788t | *Inorg. Chem.* 2012, 51, 377–385

Scheme 2. Mechanism Proposed by Torrent et al. for a $Fe(CO)_5$-Catalyzed WGSR

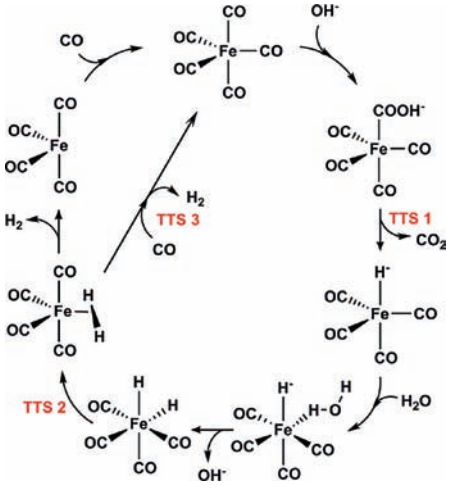

Scheme 3. Mechanism Proposed by Barrows for a $Fe(CO)_5$-Catalyzed WGSR

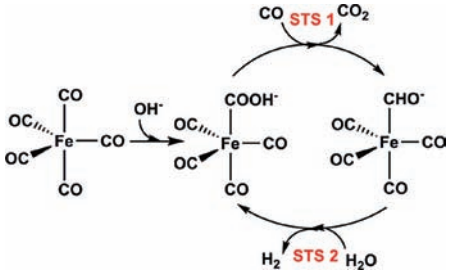

a new mechanism that included the $Fe(CO)_4H^-$ species and also excluded the OH^- desorption step (see Scheme 4).

Scheme 4. Mechanism Proposed by Rozanska and Vuilleumier for a $Fe(CO)_5$-Catalyzed WGSR

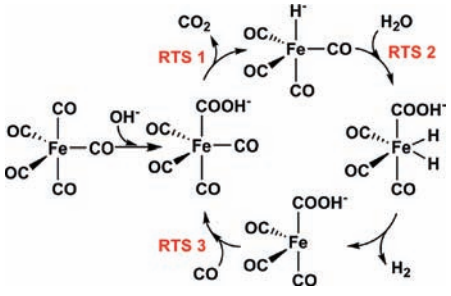

Subsequent to this, Zhang et al.[22] have done a theoretical revisit of the mechanism, examining other new possible pathways for the WGSR (see Scheme 5).

As Schemes 1−5 indicate, what all of the proposed WGSR mechanisms have in common is a mononuclear metal catalyst that does the conversion of CO and H_2O to CO_2 and H_2. However, it is of interest to note that binuclear intermediates having the formula $Fe_2(CO)_8OH^-$ [potentially $Fe_2(CO)_7COOH^-$] have been observed during gas-phase experimental studies on the $Fe(CO)_5$-catalyzed WGSR, at increased flow rates of $Fe(CO)_5$.[18] It is possible that the mononuclear $Fe(CO)_5$ species can form binuclear intermediates, and because of the consequent possibilities of metal−metal cooperativity, this may lead to a mechanistic cycle for the WGSR

Scheme 5. Mechanism Proposed by Zhang et al. for a $Fe(CO)_5$-Catalyzed WGSR

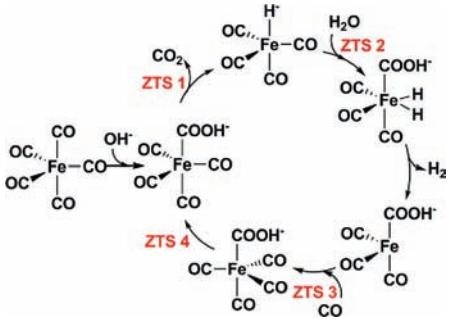

that is more energetically favorable. Indeed, metal−metal cooperativity leading to the WGSR has been observed for bimetallic ruthenium-based systems.[23,24] These considerations have led us to propose a new mechanism for the WGSR that incorporates metal−metal cooperativity and binuclear intermediates during the reaction cycle. This mechanism is shown in Scheme 6. As the scheme indicates, two $Fe(CO)_5$ molecules

Scheme 6. Newly Proposed Mechanism for a Homogeneous $Fe(CO)_5$-Catalyzed WGSR, Describing a Bimetallic Pathway

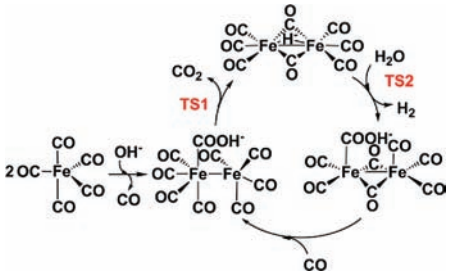

and OH^- can combine to form $Fe_2(CO)_8COOH^-$, which can then decarboxylate to yield $Fe_2(CO)_8H^-$, followed by the addition of H_2O and the loss of H_2 to yield the $Fe_2(CO)_7COOH^-$ intermediate, which upon the addition of CO would give back the $Fe_2(CO)_8COOH^-$ species and complete the cycle.

Our objective in this work has been to evaluate all of the steps of this mechanistic cycle through full gas-phase quantum mechanical (QM) calculations using density functional theory (DFT). Furthermore, we calculated all of the intermediates and transition states pertaining to all of the previous WGSR mechanisms proposed by Torrent et al.,[19] Barrows,[20] Rozanska and Vuilleumier,[21] and Zhang et al.,[22] shown in Schemes 2−5. This has been done in order to evaluate the efficiency of our mechanism in comparison to the other proposed mechanisms, at the same level of theory. Moreover, the recently designed "energetic span model" (ESM) developed by Shaik and coworkers[25−27] has been employed to determine the relative turnover frequencies (TOFs) for the different mechanisms. This has been done as a further index for comparing our proposed mechanism with the others in order to evaluate the one with the highest efficiency, that is, the one that would give the highest TOF. This is a more reliable way of comparing the different mechanisms because it takes into account not only the principal rate-determining transition state but also the other, potentially rate-influencing transition states and intermediates during the catalysis process.[25]

dx.doi.org/10.1021/ic201788t | Inorg. Chem. 2012, 51, 377−385

In addition to the gas-phase calculations, we have also reported in the manuscript the energy profiles for the different mechanisms after incorporating solvent effects. This is because it is possible that a reaction mechanism that is calculated to be energetically unfavorable in the gas phase could be found to be favorable in the solvent phase. This is due to the possibility of differential energy stabilization of the solvent on the charge dissociated ion-pair intermediates and transition states. Such differences in energy stabilization can potentially alter the energetics of the different mechanistic cycles and cause one mechanism that was less significant in the gas phase to become more predominant in the solvent phase. The possibility of this occurring has been speculated in the past.[21,28] In order to determine the relative efficacies of the different reaction mechanisms, the ESM has also been employed with the results obtained from for the solvent-phase calculations, for different solvent combinations of water and methanol. Finally, on the basis of the insights gained from our mechanistic studies, we have discussed the possibility of developing new bimetallic systems for the homogeneous catalysis of the WGSR.

COMPUTATIONAL DETAILS

Geometry optimizations and vibrational frequency calculations were performed at the level of DFT-B3LYP[29,30] in *Gaussian 09*.[31] The basis set employed was 6-31++g(d,p).[32] Previous reports[20] on WGSR mechanisms have employed this functional and basis set combination. As shown in Table S1 in the Supporting Information, the results obtained from the present calculations on the previously reported mechanisms accurately match the reported ΔE values. Further validity for the chosen basis set was provided by full geometry optimizations done for a set of structures with 6-311++g(2df,2pd). As shown in Table S2 in the Supporting Information, it was found that there was no change in the bond lengths and angles between the different structures obtained from the geometry optimizations done with the 6-31++g(d,p) and 6-311++g(2df,2pd) basis sets, thus indicating that the geometries obtained from the 6-31++g(d,p) basis set are reliable. With regard to the energies, a comparison to the experimentally observed ΔH values[17] for a given set of reactions, collected in Table S3 in the Supporting Information, indicated that the ΔH values calculated with the 6-31++g(d,p) basis set corresponded better with the experimental values than the ΔH values obtained with the 6-311++g(2df,2pd) basis set. Hence, the 6-31++g(d,p) basis set, employed for all of the calculations reported in the current manuscript, seemed to be appropriate for obtaining both reliable structures and potential energy surfaces. A further correction that was considered for the energies was a DFT-D3 dispersion correction,[33,34] done as a single-point correction to the final geometry-optimized structures. DFT-D3 dispersion corrections with zero damping and Becke–Johnson damping were considered. As shown in Table S3 in the Supporting Information, the dispersion-corrected ΔH values for a given set of reactions corresponded better with the experimental ΔH values in comparison to the uncorrected values, in some cases. However, in many cases, the uncorrected ΔH values corresponded better with the experiment than the dispersion-corrected ΔH values, for both types of dispersion corrections considered (see Table S3 in the Supporting Information). Therefore, the DFT-D3 dispersion corrections have not been included for the results for the potential energy surfaces obtained for the different reactions discussed in the manuscript.

Solvent corrections were included with the help of the PCM-SMD[35] model. The parameters that were employed when using this model were taken from the database by Truhlar and co-workers.[35,36] The values are shown in Table 1. It is to be noted that the database provides parameters only for pure solvents. Each of the seven parameters for the methanol–water mixtures has been calculated as the weighted average of the corresponding parameters of methanol and water from Truhlar's database.

Table 1. Weighted Averages for the Parameters for Different Water–Methanol Compositions, with the Parameters for Pure Water and Methanol Having Been Taken from Truhlar's Database

parameters	water	methanol	25% methanol	50% methanol	75% methanol
n	1.333	1.328	1.332	1.331	1.329
α	0.820	0.430	0.723	0.625	0.528
β	0.350	0.470	0.380	0.410	0.440
γ	0.000	31.770	7.943	15.885	23.828
ε	78.355	32.613	66.919	55.484	44.049
ϕ	0.000	0.000	0.000	0.000	0.000
ψ	0.000	0.000	0.000	0.000	0.000

The contributions of internal energy and entropy were further obtained from frequency calculations done on the DFT structures at 298.15 K: thus, the energies reported in the figures of the paper are the ΔG values. Care has been taken to ensure that all of the transition states had only one negative frequency. In this regard, it is noted that, for the solvent-corrected calculations, a correction factor in the shape of an additional 1.89 kcal/mol was added to the free energy values, in order to account for the standard solute concentration in the solvent, which is 1 M, or equivalently, 24 ATM.[37,38] The potential energy surfaces of the mechanisms described in the manuscript can be obtained for low catalyst concentrations, corresponding to 1 ATM, by subtraction of this correction factor from all of the reactant, intermediate, and product species in each of the energy profiles.

The efficiency of a catalytic cycle can be analyzed through the determination of TOFs. Shaik and co-workers[25] have proposed an ESM in order to calculate TOF from theoretically obtained energy profiles. According to this model, the TOF-determining transition state and intermediate can be located from a catalytic cycle by evaluation of the degree of TOF control (X_{TOF}).[25] TOF can be calculated by the following equation:

$$\mathrm{TOF} = \frac{K_B T}{h} e^{-\delta E/RT}$$

where δE, the energetic span, can be defined as

$$\delta E = \begin{cases} T_{TDTS} - T_{TDI} & \text{if TDTS appears after TDI} \\ T_{TDTS} - T_{TDI} + \Delta G_r & \text{if TDTS appears before TDI} \end{cases}$$

This model has been employed to calculate the TOFs for the free energy profiles obtained for the different mechanisms discussed in the paper.

RESULTS AND DISCUSSION

Proposed Binuclear Mechanism. Shown in Figure 1 is the energy profile for our proposed binuclear mechanism in the gas phase (shown in the brackets) as well as for the reaction occurring for a solvent consisting of a 50% methanol–water mixture (values shown outside the brackets). Our mechanism shows the possibility of the formation of the binuclear intermediate $Fe_2(CO)_8COOH^-$ from two mononuclear $Fe(CO)_5$ species reacting with OH^-. The formation of $Fe_2(CO)_8COOH^-$ is envisaged to occur through the following two steps: (i) the formation of the $Fe(CO)_4COOH^-$ species through the reaction of $Fe(CO)_5$ with OH^-, as described in all of the previously proposed mechanisms (see Schemes 2–5) followed by (ii) the reaction of $Fe(CO)_4COOH^-$ with another $Fe(CO)_5$ to produce $Fe_2(CO)_8COOH^-$, releasing a molecule of CO in the process. As Figure 1 indicates, the reaction is endothermic by 6.0 kcal/mol (ΔG value) in the solvent phase, while it is favorable by 44.0 kcal/mol (ΔG value) in the gas phase. The greater stabilization of the OH^- reactant species by the solvent

dx.doi.org/10.1021/ic201788t | *Inorg. Chem.* 2012, 51, 377–385

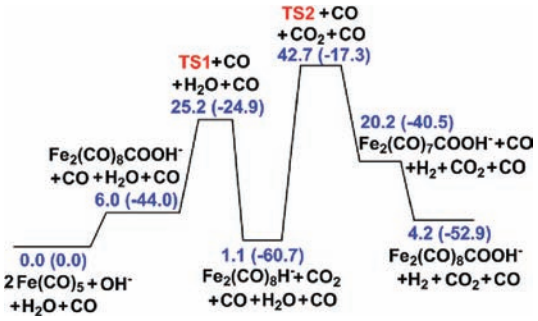

Figure 1. Free energy profile for the newly proposed mechanism using $Fe(CO)_5$ as the catalyst, which investigates a bimetallic pathway. Solvent corrections considered are for the 50% methanol–water mixture case, the gas-phase values are given in parentheses; all values are in kcal/mol.

leads to the reduced favorability of the reaction in the solvent phase. The formed $Fe_2(CO)_8COOH^-$ species can subsequently decarboxylate to produce the binuclear hydride species, $Fe_2(CO)_8H^-$, after passing through the transition state labeled as TS1 in Figure 1. The formation of a binuclear hydride intermediate species has been proposed in the past for the WGSR for the mononuclear $Ru(CO)_5$ species.[14] The transition-state structure of TS1 is shown in Figure 2a. The

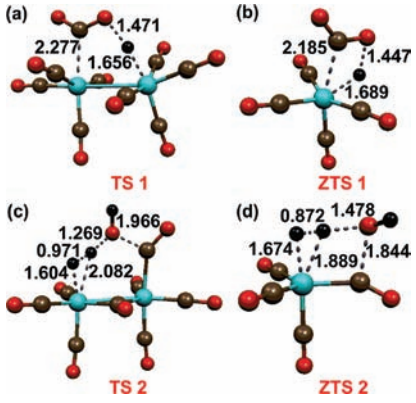

Figure 2. Optimized structures for the transition states (a) TS1, (b) ZTS1, (c) TS2, and (d) ZTS2. TS1 and TS2 correspond to the transition states obtained for the newly proposed bimetallic mechanism, while ZTS1 and ZTS2 are the transition states obtained for the Zhang mechanism. The color scheme is as follows: iron, green; carbon, brown; oxygen, red; hydrogen, black.

addition of water to the binuclear hydride $Fe_2(CO)_8H^-$ would yield $Fe_2(CO)_7COOH^-$ along with the formation of H_2 in the step with the highest activation barrier in the cycle, passing through a barrier of 41.6 kcal/mol in the solvent phase and of 43.4 kcal/mol in the gas phase. The transition state structure (TS2) for this process is shown in Figure 2c. The further addition of CO to $Fe_2(CO)_7COOH^-$ would give back the $Fe_2(CO)_8COOH^-$ species and complete the catalytic cycle.

As mentioned in the Introduction, we have also determined the free energy profiles for the reaction mechanisms proposed by Torrent et al.,[19] Barrows,[20] Rozanska and Vuilleumier,[21] and Zhang et al.,[22] and they are shown in Figures 3–6, respectively. Like in the case of Figure 1, the values inside and outside the parentheses indicate the ΔG values obtained in the gas and solvent phases, respectively, with the solvent, as before, being a 50% mixture of water and methanol. A perusal of the obtained

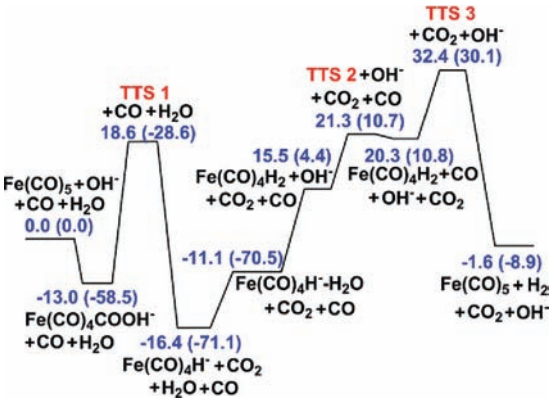

Figure 3. Free energy profile for the Torrent mechanism. Solvent corrections considered are for the 50% methanol–water mixture case; gas-phase values are given in parentheses; all values are in kcal/mol.

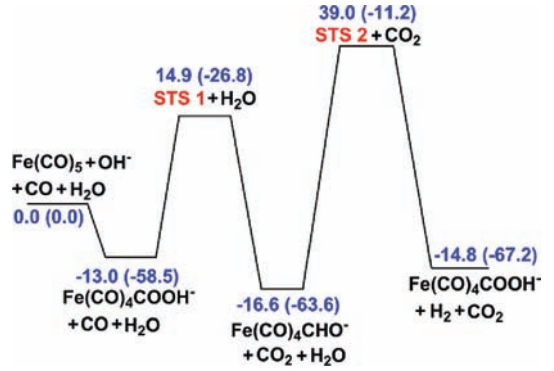

Figure 4. Free energy profile for the Barrows mechanism. Solvent corrections considered are for the 50% methanol–water mixture case; gas-phase values are given in parentheses; all values are in kcal/mol.

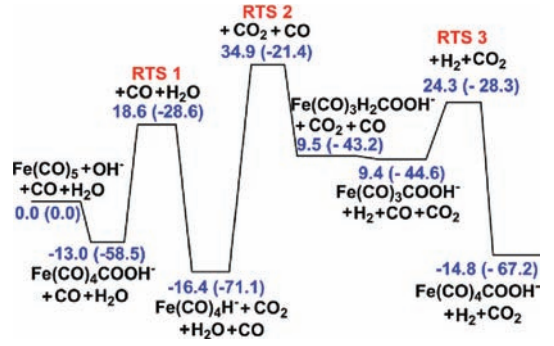

Figure 5. Free energy profile for the Rozanska–Vuilleumier mechanism. Solvent corrections considered are for the 50% methanol–water mixture case; gas-phase values are given in parentheses; all values are in kcal/mol.

ΔG values for the other mechanisms and their comparison to the values that have been obtained for our proposed binuclear mechanism indicates that the two barriers, TS1 and TS2, in our mechanism are lower than the corresponding barriers in all of the other proposed mechanisms. For the TS1 case, the transition state prior to the release of CO_2, the ΔG value for the barrier calculated in the gas (19.1 kcal/mol) and solvent (19.2 kcal/mol) phases for the binuclear mechanism is lower than the corresponding, CO_2 producing reaction barriers in the gas and solvent phases for the mechanism proposed by Torrent et al. (29.9 kcal/mol, gas phase; 31.6 kcal/mol, solvent phase),

dx.doi.org/10.1021/ic201788t | Inorg. Chem. 2012, 51, 377–385

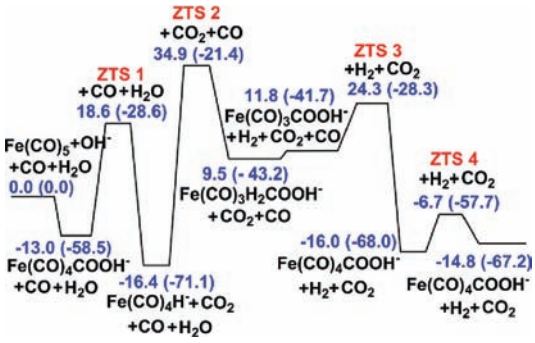

Figure 6. Free energy profile for the Zhang mechanism. Solvent corrections considered are for the 50% methanol–water mixture case; gas-phase values are given in parentheses; all values are in kcal/mol.

by Barrows (31.7 kcal/mol, gas phase; 27.9 kcal/mol, solvent phase), by Rozanska and Vuilleumier (29.9 kcal/mol, gas phase; 31.6 kcal/mol, solvent phase), and by Zhang et al. (29.9 kcal/mol, gas phase; 31.6 kcal/mol, solvent phase) (see Figures 1 and 3–6). Likewise, for TS2, the binuclear mechanism, the values (43.4 kcal/mol, gas phase; 41.6 kcal/mol, solvent phase) are lower than the values obtained for the H_2 formation step, the step with the highest activation barrier, by Torrent et al. (101.2 kcal/mol, gas phase; 48.8 kcal/mol, solvent phase), by Barrows (52.4 kcal/mol, gas phase; 55.6 kcal/mol, solvent phase), by Rozanska and Vuilleumier (49.7 kcal/mol, gas phase; 51.3 kcal/mol, solvent phase), and by Zhang et al. (49.7 kcal/mol, gas phase; 51.3 kcal/mol, solvent phase) (see Figures 1 and 3–6). The reason why the binuclear mechanism provides more facile transformations through lower barriers is explained by the metal–metal cooperativity between the two iron centers. Figure 2 shows the structures of the transition states that have been obtained from the binuclear mechanism: TS1 (Figure 2a) and TS2 (Figure 2c) as well as the corresponding transition state structures (Figure 2b,d) obtained from the mononuclear Zhang mechanism, indicated as ZTS1 and ZTS2 and shown for the purpose of comparison. A comparison of TS1 and ZTS1 shows that the presence of two iron centers in TS1 makes a five-membered ring, which is less sterically crowded and therefore more favorable than the more highly strained four-membered ring formed in the case of ZTS1. Similarly, TS2 is a more sterically favored six-membered ring structure in comparison to the more encumbered five-membered ring ZTS2 structure. The formation of a five-membered transition state leading to a more facile reaction for a bimetallic species in comparison to a mononuclear one had been observed earlier, for the case of alkene insertion into the C–H bond, for a ytterbium-based catalyst.[39] The formation of the binuclear species thus alleviates ring strain in both transition states and leads to lower barriers. It appears that it is this steric advantage conferred by metal–metal cooperativity that is the principal cause of the lower barriers for the binuclear mechanism: a natural bond orbital (NBO)[40] analysis, conducted for the intermediates and transition states for both the binuclear and Zhang mechanisms, did not reveal any significant differences in the essential nature of the bonding between the atoms in the intermediates and transition states. The charges obtained from the NBO analysis for the intermediates and transition states TS2 and ZTS2 are shown in Table S4 in the Supporting Information.

Comparison of the Efficiency of the Different Mechanisms Using the ESM. As discussed in the Introduction, the efficiency of the different mechanisms has been further compared with the help of TOF calculations done with the aid of the ESM.[25] This is a more reliable way of comparing the different mechanisms because it takes into account not only the principal rate-determining transition state but also the other, potentially rate-influencing transition states and intermediates during the catalysis process. Discussed in this section are the TOFs calculated for the different reaction mechanisms, not only in the gas phase but also in the solvent phase for different methanol–water mixture combinations. We have analyzed the effect of 25%, 50%, and 75% methanol–water mixtures computationally using Truhlar's database.[36] The calculated free energy profiles for the 25% and 75% methanol–water mixtures are provided in the Supporting Information (see Figures S1–S5).

A perusal of the mechanistic cycles shown in Figures 3–6 indicates that the mononuclear mechanisms have shared intermediates and transition states. Moreover, all of the mechanisms shown in Figures 1 and 3–6 compare mechanistic routes starting from the same catalyst: $Fe(CO)_5$. Therefore, according to the ESM, if one accessible state has very low energy, it will be the TOF-determining intermediate (TDI) for *all* of the mechanisms. This is also true when it comes to evaluating the TOF-determining transition state (TDTS) for the ESM calculations. Therefore, it is necessary to compare the energy profiles for all of the mechanisms, in both the gas and solvent phases, in order to find the TDI and TDTS for each case. Figure 7 shows the different energy profiles for the

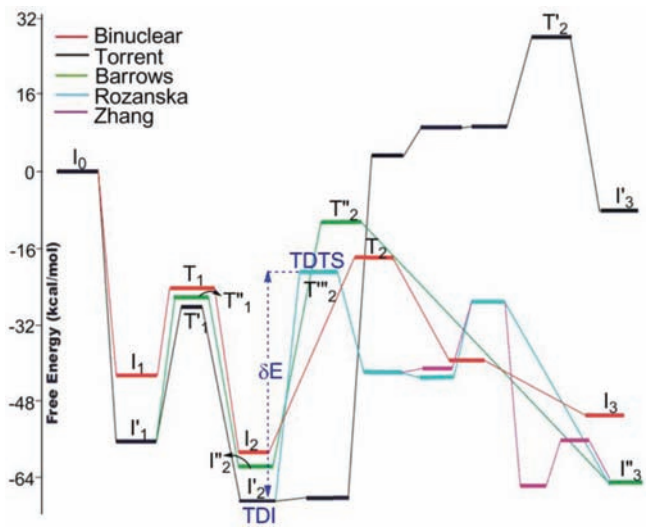

Figure 7. Combined free energy profile of all of the $Fe(CO)_5$-catalyzed mechanisms in the gas phase.

mechanistic cycles considered in the gas phase. Shown in blue are the lowest lying intermediate and transition state for the gas-phase calculations, which would be the TDI and TDTS for the WGSR in the gas phase when using the $Fe(CO)_5$ catalyst. As Figure 7 indicates, both the TDI and TDTS correspond to the Zhang mechanism. The newly proposed binuclear mechanism has a lower *difference* between its intermediates and transition states (barrier heights), as shown in the previous section, but it does not yield the lowest intermediate or transition state along the potential energy surface. Therefore, even though the effects of metal–metal cooperativity enable the binuclear mechanism to have lower barriers in the mechanistic cycle, the fact that the intermediates and transition states in this mechanistic cycle lie slightly higher than those for the

dx.doi.org/10.1021/ic201788t | *Inorg. Chem.* 2012, 51, 377–385

competing mononuclear mechanistic cycles leads to it not being the predominant mechanism for the $Fe(CO)_5$ catalyst and thus not contributing to the TDI or TDTS in the ESM TOF calculations.

The same results are obtained when considering the potential energy surfaces for the solvent-corrected potential energy surfaces for the different mechanistic cycles. Shown in Figure 8

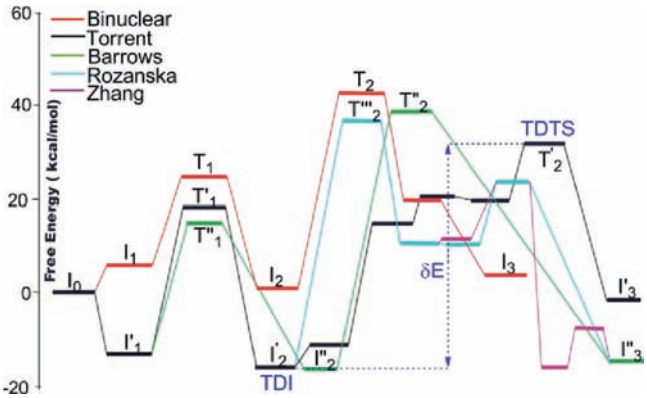

Figure 8. Solvent-corrected combined free energy profile of all of the $Fe(CO)_5$-catalyzed mechanisms, for the case of the 50% methanol–water mixture. All values are in kcal/mol.

is a comparison of the potential energy surfaces of the intermediates and transition states for the different WGSR mechanisms for the solvent-corrected energies pertaining to the case of the 50% water–methanol mixture solvent. For this case (as well as for the 25% and 75% water–methanol mixture cases), it is the mononuclear Torrent mechanism that was found to yield the TDI and TDTS (shown in blue; see Figure 8). In this regard, it is to be noted that, for the TDI, the Barrows mechanism does have a slightly lower intermediate—lower by only 0.2 kcal/mol—than the Torrent mechanism intermediate that has been chosen for the TDI. However, the Barrows mechanism intermediate has not been considered as the TDI because this does not connect to the TDTS (obtained from the Torrent mechanism) through a shared pathway. Because the difference between the Torrent intermediate and the Barrows intermediate is small enough (0.2 kcal/mol) to fall within the bounds of the systematic calculation error, the Torrent mechanism intermediate has been considered the TDI for the ESM calculations. Again, as for the gas-phase results, the newly proposed binuclear mechanism, despite having lower barrier heights did not contribute to the TDI or TDTS because its intermediates and transition states were found to lie higher in energy than the corresponding intermediates and transition states for the Torrent mechanism.

Having determined the TDI and TDTS for the different gas- and solvent-phase (25%, 50%, and 75% methanol–water mixtures) cases, the TOF calculations were then done for each case. The results are collected in Table 2. The first row of

Table 2. Absolute and Relative TOF Values (h^{-1}) Obtained for the Mononuclear Mechanism Using $Fe(CO)_5$ as the Catalyst

	gas phase	25% methanol	50% methanol	75% methanol
absolute TOF	7.5×10^{-21}	4.8×10^{-20}	3.5×10^{-20}	3.5×10^{-20}
relative TOF	1.0	6.4	4.7	4.7

TOF values in Table 2 shows the absolute values of the calculated TOFs for the overall mechanistic cycles derived for the gas phase and the different solvent mixture cases. As seen in Table 2, the absolute TOF values are on the order of 10^{-20}, but this is likely due to the sensitivity of the method to error when the exponential terms are compared. It is, however, to be noted that the value of the ESM TOF calculations lies in a comparison of the *relative* TOF values rather than *absolute* TOF numbers, especially (as in the current calculations) when all of the values for the barrier heights and the energies of the intermediates have been calculated at the same level of theory. The errors arising from a comparison of the exponential terms are compensated for when doing relative TOF comparisons.[25] The relative TOF values, shown in the second row of Table 2, were obtained by dividing all of the entries for the absolute TOF values by the smallest TOF value: 7.5×10^{-21} h^{-1}, obtained for the gas-phase calculation.

As seen in Table 2, the comparison of the relative TOF values for the different cases provides some useful insights into the nature of the mechanisms for the WGSR. These are discussed pointwise below:

(i) As was mentioned in the Introduction, one of the reasons for incorporating solvent corrections was to determine whether certain mechanistic cycles that had been found to be less significant in the gas phase would become more important once solvent effects were introduced. As seen from the composite mechanism derived from the different mechanisms for the solvent case shown in Figure 8 (50% methanol–water mixture), this is indeed true for the Torrent mechanism, which is seen to provide the TDI and TDTS for the ESM calculations in the solvent phase, while the transition states for the same Torrent mechanism in the gas phase were found to lie significantly higher in energy than those for the other competing mechanisms (see Figure 7). The reason for this is because the Torrent mechanism is the only one among all of the proposed mechanisms that involves desorption of OH^- in one of the intermediate stages (see Scheme 2 and Figure 3). While desorption of OH^- is a highly endothermic process in the gas phase (75.5 kcal/mol), it is much more favored in the solvent phase (31.9 kcal/mol for the case of the 50% methanol–water mixture) because of the greater degree of stabilization of the small OH^- ion by the solvent. Thus, the results validate the need to check all of the proposed mechanisms, even ones that had been found to be very poor in the gas phase, once solvent corrections had been added.

(ii) The absolute, as well as the relative, TOF values calculated for the WGSR mechanisms in the different solvent mixture cases indicate that the efficiency of the WGSR decreases with an increase of the percent of methanol in the methanol–water mixtures (see Table 2): the relative TOF value is 6.4 for the 25% methanol–water mixture, while it is 4.7 for both the 50% and 75% methanol–water mixtures. This appears to contradict experimental observations: different methanol–water mixtures have been experimentally studied by King and co-workers,[9] who have found that the efficiency of the WGSR improved at higher methanol–water ratios. This discrepancy between the experimental and computational results can be explained by the fact that methanol acts not only as a solvent but also as a reactant for the WGSR,

dx.doi.org/10.1021/ic201788t | *Inorg. Chem.* 2012, 51, 377–385

providing the OH^- ions that are necessary for the formation of the important $Fe(CO)_4COOH^-$ intermediate species in the mononuclear mechanism and the $Fe_2(CO)_8COOH^-$ intermediate species in the proposed binuclear mechanism. As a solvent, increased methanol in the methanol–water mixtures would reduce the dielectric constant of the solvent and thus act to reduce stabilization of the ionic intermediates and transition states, which gets reflected in the lower TOF values shown in Table 2. However, as a reactant, increased methanol in the methanol–water mixtures would improve the efficiency of the WGSR and lead to increased TOF because of the increased availability of OH^- during the reaction. Thus, the experimentally observed favorable effect of increased methanol in methanol–water mixtures[9] suggests that methanol in its role as a reactant has a greater influence on the WGSR than in its role as a solvent.

(iii) Finally, a perusal of the energy profiles in Figures 7 and 8, as well as the fact that the composite mechanism determined for the gas-phase and solvent mixture cases does not include any TDI or TDTS from the newly proposed binuclear mechanism, shows that the effects of metal–metal cooperativity would not have an impact on the rate or the TOF for the WGSR when using the $Fe(CO)_5$ catalyst. The reason for this is the fact that the first step of the binuclear mechanism involves a dimerization process: the reaction of two $Fe(CO)_5$ molecules with OH^- to form the $Fe_2(CO)_8COOH^-$ species. Such a process is entropically disfavored, and this is reflected in the higher energy of the first intermediate in comparison to the other intermediates in the other mechanisms. This entropic unfavorability may provide an explanation for why the binuclear species having the formula $Fe_2(CO)_8OH^-$ [likely to be $Fe_2(CO)_7COOH^-$] has only been experimentally observed at increased flow rates of $Fe(CO)_5$.[18] What is important to note, however, is that the problem of entropic unfavorability would not exist for iron-based catalysts *that are binuclear to begin with*. In such a situation, the first unfavorable dimerization step is automatically avoided, and then one might see the advantages of metal–metal cooperativity, leading to significant improvements in the TOF. This is discussed further in the next section.

Designing Improved Catalysts for the WGSR. As pointed out at the end of the previous section, the true potential of metal–metal cooperativity in improving the yield from the WGSR can be realized if one designed bimetallic systems, thereby eliminating the entropically unfavorable dimerization step necessary for the binuclear mechanism when employing monometallic catalysts. This point is made more clear through the example of the binuclear complex $Fe_2(CO)_9$ considered as the catalyst for the WGSR. Shown in Figure 9 is the free energy profile for the gas- and solvent-phase (50% methanol–50% water) catalysis of the WGSR by $Fe_2(CO)_9$. As the figure indicates, the formation of the $Fe_2(CO)_8COOH^-$ species for this case is now an exergonic process in both the gas phase [$\Delta G = -73.6$ kcal/mol, 29.6 kcal/mol more stable than that for the binuclear mechanism with the $Fe(CO)_5$ catalyst] and the solvent phase [$\Delta G = -16.9$ kcal/mol, 22.9 kcal/mol more stable than that for the binuclear

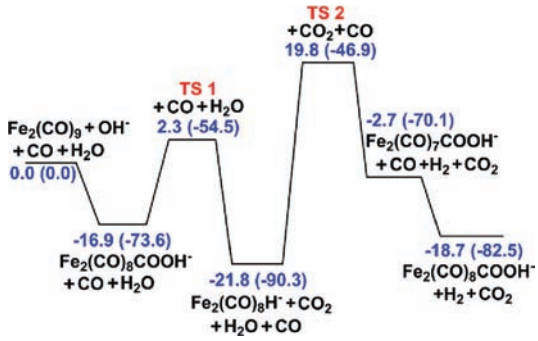

Figure 9. Free energy profile for the newly proposed mechanism for the bimetallic $Fe_2(CO)_9$ catalyst, with the 50% methanol–water mixture as the solvent. Gas-phase values are given in parentheses; all values are in kcal/mol.

mechanism with the $Fe(CO)_5$ catalyst]. This leads to a significantly increased overall energetic favorability for the entire reaction cycle: the completion of the cycle is now exergonic by 82.5 kcal/mol in the gas phase compared to it being only exergonic by 52.9 kcal/mol for the binuclear mechanism with the $Fe(CO)_5$ catalyst. It is noted here that $Fe_2(CO)_9$ is only used as an example: its insolubility in methanol makes it an unlikely candidate for a binuclear WGSR catalyst. It is also to be noted that the bimetallic catalyst to be employed for the WGSR should be resistant to dissociation to yield mononuclear species during the WGSR catalysis because this would again lead to the predominance of mononuclear mechanisms over binuclear mechanisms, as was previously shown in Figures 7 and 8.

A comparison of the TDI and TDTS for the bimetallic $Fe_2(CO)_9$ catalyst to the TDI and TDTS obtained for the mononuclear $Fe(CO)_5$ catalyst in the gas phase (Figure 10) and

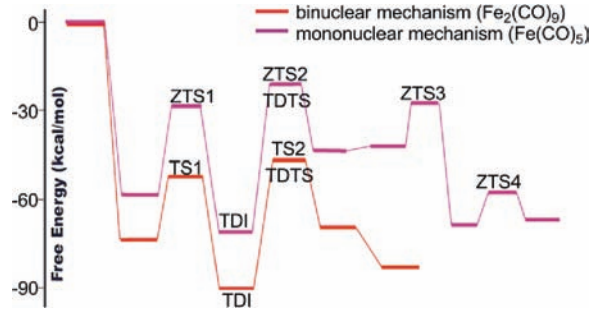

Figure 10. Comparison of the free energy profiles in the gas phase obtained with $Fe(CO)_5$ and $Fe_2(CO)_9$ as the catalysts.

the solvent phase (50% methanol–water mixture; Figure 11) suggests that the bimetallic catalyst would perform significantly better. This is also true for the other two solvent mixture cases considered: the 25% methanol–water mixture and the 75% methanol–water mixture cases, the free energy profiles of the bimetallic mechanism for which have been included as Figure S6 in the Supporting Information. The superior performance of the bimetallic catalyst is further illustrated from calculation of the relative TOF values for the gas phase and the different solvent mixture cases that have been collected and shown in Table 3. The relative TOF values were calculated by dividing the absolute TOF values obtained for the bimetallic $Fe_2(CO)_9$ catalyst by the corresponding absolute TOF value obtained for the mononuclear $Fe(CO)_5$ catalyst for each of the cases

dx.doi.org/10.1021/ic201788t | *Inorg. Chem.* 2012, 51, 377–385

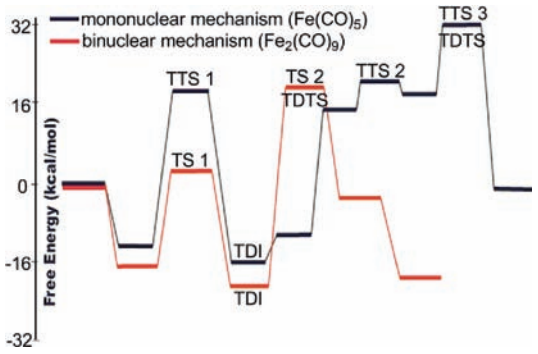

Figure 11. Comparison of the free energy profiles obtained for the case of the 50% methanol–water mixture, with $Fe(CO)_5$ and $Fe_2(CO)_9$ as the catalysts.

considered (the absolute TOF values for each case are provided in Table S5 in the Supporting Information). It is clear from the relative TOF values obtained that the bimetallic catalyst species would provide a performance that would be at least 2 orders of magnitude better than that of the monometallic species (see Table 3). Thus, the advantages of metal–metal

Table 3. Relative TOF Values, Obtained for the Mononuclear $Fe(CO)_5$ and Binuclear $Fe_2(CO)_9$ Catalysts, in the Gas Phase and for the Different Solvent Mixture Cases

mechanism	gas phase	25% methanol	50% methanol	75% methanol
mononuclear $Fe(CO)_5$ catalyst	1.0	1.0	1.0	1.0
binuclear $Fe_2(CO)_9$ catalyst	4.3×10^4	2.7×10^5	1.9×10^5	9.7×10^4

cooperativity in reducing the barriers for the WGSR that have been uncovered through the work discussed here provide a guide for the design of improved WGSR catalysts in the future.

CONCLUSIONS

Computational studies employing DFT have been done in order to investigate a binuclear mechanism for the homogeneous WGSR. This represents the first mechanistic computational investigations of metal–metal cooperativity for the WGSR. A binuclear mechanism has been proposed for the WGSR with the $Fe(CO)_5$ catalyst and compared with full QM calculations with all of the previously suggested mechanisms[19−22] in the literature. The calculations indicate that the binuclear mechanism leads to lower barriers in comparison to the previously proposed mononuclear mechanisms. While the comparison of the free energy profiles, as well as the predicted TOFs, with the aid of the recently developed ESM,[25] indicates that the binuclear mechanism would not be the predominant mechanism if one were to start from a mononuclear catalyst, calculations indicate that one would achieve much higher TOFs if a bimetallic rather than a mononuclear catalyst was to be employed for the WGSR. It is, however, important to note that this would only be true provided the bimetallic species does not dissociate to a lower energy monometallic species during the catalysis process. While the calculations have been done with iron-based catalysts, a natural extension of the results obtained here is the prediction that metal–metal cooperativity would be likely to render other bimetallic catalysts, such as biruthenium systems, for instance, more effective than their mononuclear counterparts in catalyzing the WGSR. The calculations thus provide a recipe for the design of better WGSR catalysts in the future: soluble bimetallic complexes that can exploit metal–metal cooperativity in order to increase the efficiency of WGSR catalysis.

ASSOCIATED CONTENT

Supporting Information

Comparison of the ΔE values of the current calculation with the previously reported ΔE values (Table S1) using the same basis set, comparison of the geometries with different basis sets (Table S2), comparison of the ΔH values obtained from different computational calculations with the experimental ΔH values for a set of reactions (Table S3), free energy profiles for the 25% and 75% methanol–water mixtures (Figures S1–S6), natural charges from NBO analysis (Table S4), absolute TOFs (h^{-1}) (Table S5), and the *xyz* coordinates of all of the structures. This material is available free of charge via the Internet at http://pubs.acs.org.

AUTHOR INFORMATION

Corresponding Author

*E-mail: k.vanka@ncl.res.in. Fax: (+) 020-2590-2636.

ACKNOWLEDGMENTS

The authors acknowledge the Centre of Excellence in Scientific Computing, NCL, Pune, India, for providing computational resources. The financial support of the Council of Scientific and Industrial Research (CSIR), New Delhi, through the network programme NWP-0022-I as well as the Department of Science and Technology, India, is gratefully acknowledged. N.K. acknowledges UGC for providing a research fellowship. The authors also acknowledge K. R. Aswathy and Prakash Chandra for performing preliminary test calculations on the $Fe(CO)_5$-catalyzed WGSR system.

REFERENCES

(1) Motta, A.; Fragala, I. L.; Marks, T. J. *J. Am. Chem. Soc.* **2009**, *131*, 3974–3984.
(2) Torkelson, J. R.; Antwi-Nsiah, F. H.; McDonald, R.; Cowie, M.; Pruis, J. G.; Jalkanen, K. J.; DeKock, R. L. *J. Am. Chem. Soc.* **1999**, *121*, 3666–3683.
(3) Wigginton, J. R.; Chokshi, A.; Graham, T. W.; McDonald, R.; Ferguson, M. J.; Cowie, M. *Organometallics* **2005**, *24*, 6398–6410.
(4) Miller, A. E. S.; Beauchamp, J. L. *J. Am. Chem. Soc.* **1991**, *113*, 8765–8770.
(5) Kang, H. C.; Mauldin, C. H.; Cole, T.; Slegeir, W.; Cann, K.; Pettit, R. *J. Am. Chem. Soc.* **1977**, *99*, 8323–8325.
(6) King, A. D.; King, R. B.; Yang, D. B. *J. Am. Chem. Soc.* **1981**, *103*, 2699–2704.
(7) King, R. B.; Frazier, C. C.; Hanes, R. M.; King, A. D. *J. Am. Chem. Soc.* **1978**, *100*, 2925–2927.
(8) Reppe, J. W.; Reindl, E. *Liebigs Ann. Chem.* **1953**, *582*, 121–124.
(9) King, A. D.; King, R. B.; Yang, D. B. *J. Am. Chem. Soc.* **1980**, *102*, 1028–1032.
(10) Lane, K. R.; Sallans, L.; Squires, R. R. *Organometallics* **1985**, *4*, 408–410.
(11) Kunkes, E. L.; Simonetti, D. A.; West, R. M.; Serrano-Ruiz, J. C.; Gartner, C. A.; Dumesic, J. A. *Science* **2008**, *322*, 417–421.
(12) Serrano-Ruiz, J. C.; West, R. M.; Dumesic, J. A. *Annu. Rev. Chem. Biomol. Eng.* **2010**, *1*, 79–100.
(13) Huber, G. W.; Shabaker, J. W.; Dumesic, J. A. *Science* **2003**, *300*, 2075–2077.
(14) Ford, P. C. *Acc. Chem. Res.* **1981**, *14*, 31–37.

(15) King, A. D.; King, R. B.; Yang, D. B. *J. Chem. Soc., Chem. Commun.* **1980**, 529−530.
(16) Grice, N.; Kao, S. C.; Pettit, R. *J. Am. Chem. Soc.* **1979**, *101*, 1627−1628.
(17) Sunderlin, L. S.; Squires, R. R. *J. Am. Chem. Soc.* **1993**, *115*, 337−343.
(18) Lane, K. R.; Lee, R. E.; Sallans, L.; Squires, R. R. *J. Am. Chem. Soc.* **1984**, *106*, 5767−5772.
(19) Torrent, M.; Sola, M.; Frenking, G. *Organometallics* **1999**, *18*, 2801−2812.
(20) Barrows, S. E. *Inorg. Chem.* **2004**, *43*, 8236−8238.
(21) Rozanska, X.; Vuilleumier, R. *Inorg. Chem.* **2008**, *47*, 8635−8640.
(22) Zhang, F.; Zhao, L.; Xu, C.; Chen, Y. *Inorg. Chem.* **2010**, *49*, 3278−3281.
(23) Majumdar, M.; Sinha, A.; Ghatak, T.; Patra, S. K.; Sadhukhan, N.; Rahaman, S. M. W.; Bera, J. K. *Chem.—Eur. J.* **2010**, *16*, 2574−2585.
(24) Sinha, A.; Ghatak, T.; Bera, J. K. *Dalton Trans.* **2010**, *39*, 11301−11313.
(25) Kozuch, S.; Shaik, S. *Acc. Chem. Res.* **2010**, *44*, 101−110.
(26) Kozuch, S.; Martin, J. M. L. *ACS Catal.* **2011**, *1*, 246−253.
(27) Uhe, A.; Kozuch, S.; Shaik, S. *J. Comput. Chem.* **2010**, *32*, 978−985.
(28) Amovilli, C.; Floris, F. M.; Sola, M.; Tomasi, J. *Organometallics* **2001**, *20*, 1310−1316.
(29) Axel, D. B. *J. Chem. Phys.* **1993**, *98*, 5648−5652.
(30) Lee, C.; Yang, W.; Parr, R. G. *Phys. Rev. B* **1988**, *37*, 785.
(31) Frisch, M. J.; Trucks, G. W.; Schlegel, H. B.; Scuseria, G. E.; Robb, M. A.; Cheeseman, J. R.; Scalmani, G.; Barone, V.; Mennucci, B.; Petersson, G. A.; Nakatsuji, H.; Caricato, M.; Li, X.; Hratchian, H. P.; Izmaylov, A. F.; Bloino, J.; Zheng, G.; Sonnenberg, J. L.; Hada, M.; Ehara, M.; Toyota, K.; Fukuda, R.; Hasegawa, J.; Ishida, M.; Nakajima, T.; Honda, Y.; Kitao, O.; Nakai, H.; Vreven, T.; Montgomery, J. A., Jr.; Peralta, J. E.; Ogliaro, F.; Bearpark, M.; Heyd, J. J.; Brothers, E.; Kudin, K. N.; Staroverov, V. N.; Kobayashi, R.; Normand, J.; Raghavachari, K.; Rendell, A.; Burant, J. C.; Iyengar, S. S.; Tomasi, J.; Cossi, M.; Rega, N.; Millam, J. M.; Klene, M.; Knox, J. E.; Cross, J. B.; Bakken, V.; Adamo, C.; Jaramillo, J.; Gomperts, R.; Stratmann, R. E.; Yazyev, O.; Austin, A. J.; Cammi, R.; Pomelli, C.; Ochterski, J. W.; Martin, R. L.; Morokuma, K.; Zakrzewski, V. G.; Voth, G. A.; Salvador, P.; Dannenberg, J. J.; Dapprich, S.; Daniels, A. D.; Farkas, Ö.; Foresman, J. B.; Ortiz, J. V.; Cioslowski, J.; Fox, D. J. *Gaussian 09*, revision B.01; Gaussian, Inc.: Wallingford, CT, 2009.
(32) Ditchfield, R.; Hehre, W. J.; Pople, J. A. *J. Chem. Phys.* **1971**, *54*, 724−728.
(33) Stefan, G.; Jens, A.; Stephan, E.; Helge, K. *J. Chem. Phys.* **2010**, *132*, 154104.
(34) Grimme, S.; Ehrlich, S.; Goerigk, L. *J. Comput. Chem.* **2011**, *32*, 1456−1465.
(35) Marenich, A. V.; Cramer, C. J.; Truhlar, D. G. *J. Phys. Chem. B* **2009**, *113*, 6378−6396.
(36) Winget, P.; Dolney, D. M.; Giesen, D. J.; Cramer, C. J.; Truhlar, D. G. *Minnesota Solvent Descriptor Database*. Version date: July 9, 1999. Updated: June 6, 2010.
(37) Harvey, J. N. *Faraday Discuss.* **2009**, *145*, 487−505.
(38) Ho, J.; Klamt, A.; Coote, M. L. *J. Phys. Chem. A* **2010**, *114*, 13442−13444.
(39) Luo, Y.; Hou, Z. *Organometallics* **2006**, *25*, 6162−6165.
(40) Glendening, E. D.; Reed, A. E.; Carpenter, J. E. Weinhold, F. *NBO*, version 3.1.